ICHEP'98 #239
Submitted to Pa 7, 8
Pl 9, 10

DELPHI 98-119 CONF 180
22 June, 1998

Measurement of the B Semileptonic Branching Fraction into Orbitally Excited Charm Mesons

Preliminary

DELPHI Collaboration

D. Bloch [1], **P. Juillot** [1], **P. Roudeau** [2], **R. Strub** [1]

Abstract

A study of b semileptonic decays into orbitally excited charm mesons $D^{**0} \to D^{*+}\pi^-$ is presented. The D^{*+} mesons are exclusively reconstructed in the DELPHI experiment at LEP. A fit to the $D^{*+}\pi^-$ invariant mass spectrum allows to measure the B^- semileptonic branching fraction into the narrow D_1^0 orbital state:

$$BR(B^- \to D_1^0 \ell^- \bar{\nu}_\ell) \quad = \quad (0.72 \pm 0.22\,(\text{stat.}) \pm 0.13\,(\text{syst.}))\,\% \,.$$

A fit of the π^- impact parameter distribution provides a measurement of the B^- semileptonic branching fraction into both narrow and wide excited states:

$$BR(B^- \to D^{*+}\pi^-\ell^-\bar{\nu}_\ell X) = (1.15 \pm 0.17\,(\text{stat.}) \pm 0.14\,(\text{syst.})\,\% \,.$$

Paper submitted to the ICHEP'98 Conference
Vancouver, July 22-29

[1] Institut de Recherches Subatomiques, Strasbourg, France
[2] Laboratoire de l'Accélérateur Linéaire, Orsay, France

1 Introduction

The study of $\overline{\mathrm{B}}$ meson semileptonic decays into orbitally excited charm mesons or non-resonant $\mathrm{D}^{(*)}\pi$ final states [1] is interesting for several reasons.

First, only 60% to 70% of $\overline{\mathrm{B}}$ semileptonic decays are described by $\mathrm{D}\ell^-\bar{\nu}_\ell$ and $\mathrm{D}^*\ell^-\bar{\nu}_\ell$ final states [1]. The remaining contribution could be attributed to the production of D^{**}. The ALEPH measurement of the $\mathrm{D}^{**}\ell^-\bar{\nu}_\ell$ branching fraction does not fully account for the observed discrepancy [2].

Then, concerning the narrow orbital excitations, OPAL observed both D_1 and D_2^* states [3], whereas ALEPH and CLEO observed only the D_1 resonance [2, 4].

Finally, the ratio of branching fractions of $\overline{\mathrm{B}}$ decays into $\mathrm{D}^{*+}\pi^-\ell^-\bar{\nu}_\ell$ over all $\mathrm{D}^{*+}\ell^-$ final states is a significant contribution to the systematic uncertainty on $\tau_{\mathrm{B}^0_\mathrm{d}}$, Δm_d [5] or V_cb measurements [6].

This paper describes a search for narrow and wide orbital charm excitations in $\overline{\mathrm{B}}$ semileptonic decays in the DELPHI experiment at LEP. Only $\mathrm{D}^{*+}\pi^-\ell^-$ final states are considered where the D^{*+} are exclusively reconstructed [2]. Two analyses are performed: the first one relies on the $\mathrm{D}^{*+}\pi^-$ invariant mass distribution in order to measure the narrow resonances; the second is based on the impact parameter of the π^- candidate relative to the primary interaction vertex and aims to look for both narrow and wide D^{**} states. The present experimental and theoretical pattern of orbitally excited charm mesons is displayed in table 1.

	$J^P\ j_\mathrm{q}$		Mass (MeV/c^2)	Γ Width (MeV/c^2)	Decay modes
D_0^*	$0^+\ 1/2$		~ 2360	≥ 170	$(\mathrm{D}\pi)$
D_1^*	$1^+\ 1/2$		~ 2430	≥ 250	$(\mathrm{D}^*\pi)$
D_1	$1^+\ 3/2$	D_1^+	2427 ± 5	28 ± 8	$\mathrm{D}^{*0}\pi^+$ $(\mathrm{D}^{*+}\pi^0,\ \mathrm{D}\rho,\ \mathrm{D}\pi\pi)$
		D_1^0	2422.2 ± 1.8	$18.9^{+4.6}_{-3.5}$	$\mathrm{D}^{*+}\pi^-$ $(\mathrm{D}^{*0}\pi^0,\ \mathrm{D}\rho,\ \mathrm{D}\pi\pi)$
D_2^*	$2^+\ 3/2$	D_2^{*+}	2459 ± 4	25^{+8}_{-7}	$\mathrm{D}^0\pi^+,\ \mathrm{D}^{*0}\pi^+$ $(\mathrm{D}^{(*)+}\pi^0,\ \mathrm{D}^*\rho,\ \mathrm{D}^*\pi\pi)$
		D_2^{*0}	2458.9 ± 2.0	23 ± 5	$\mathrm{D}^+\pi^-,\ \mathrm{D}^{*+}\pi^-$ $(\mathrm{D}^{(*)0}\pi^0,\ \mathrm{D}^*\rho,\ \mathrm{D}^*\pi\pi)$

Table 1: Expected and observed orbital excitations of D^0 and D^+ mesons. The broad $j_\mathrm{q} = 1/2$ states are estimated according to [7, 8]. The narrow $j_\mathrm{q} = 3/2$ states are measured [1]. In the last column, the predicted decay modes which have not yet been observed are indicated within parentheses.

[1] Hereafter both processes are conventionally denoted as D^{**}.

[2] Throughout the paper charge-conjugate states are implicitly included; ℓ indicates an e or a μ mode, not a sum over these modes.

2 The DELPHI detector

The DELPHI detector has been described in detail elsewhere [9]; only the detectors relevant to the present analysis are briefly described in the following. The tracking of charged particles is accomplished in the barrel region with a set of cylindrical tracking detectors whose axis is oriented along the 1.23 T magnetic field and the direction of the beam. The Vertex Detector (VD) has an intrinsic resolution of 5–6 μm and consists of three concentric layers of silicon microstrip detectors at average radii of 6.3 cm, 9 cm, and 11 cm. The VD surrounds a Beryllium beam pipe with a radius of 5.5 cm. In 1991-1993 all the VD layers were single-sided with strips parallel to the beam direction. In 1994 and 1995, the inner-most and the outer-most layers were replaced by double-sided silicon microstrip modules. The Inner Detector is placed outside the VD between radii of 12 cm and 28 cm. It consists of a jet chamber giving up to 24 spatial measurements and a trigger chamber providing a measurement of the z coordinate. The VD and ID are surrounded by the main DELPHI tracking chamber, the Time Projection Chamber (TPC), which provides up to 16 space points between radii of 30 cm and 122 cm. The Outer Detector (OD) at a radius of 198 cm to 206 cm consists of five layers of drift cells. The average momentum resolution of the tracking system is $\sigma(p)/p \;=\; 0.0006\; p$ (GeV/c) for high momentum particles, in the polar region between 30^o and 150^o. The asymptotic precision to extrapolate tracks to the collision point was measured as 26 ± 2 μm using muons from Z$\rightarrow \mu^+\mu^-$. In hadronic events, the extrapolation accuracy was found to be $\sqrt{26^2 + 69^2/p_t^2}$ μm [10] where p_t is the momentum of the particle in the plane transverse to the beam axis. The tracking in the forward ($11^\circ < \theta < 33^\circ$) and backward ($147^\circ < \theta < 169^\circ$) regions is improved by two pairs of Forward drift Chambers (FCA and FCB) in the end-caps.

Hadrons are identified using the specific ionization (dE/dx) in the TPC and the Cherenkov radiation in the barrel Ring Imaging CHerenkov detector (RICH) placed between the TPC and the OD detectors.

The muon identification relies mainly on the muon chambers, a set of drift chambers with three-dimensional information situated at the periphery of DELPHI after approximately 1 m of iron. The muon identification algorithm is described in Ref. [9]. A loose selection criterion provides an identification efficiency of $(90 \pm 2)\%$ for a misidentification probability of 1.2% within the acceptance of the muon chambers.

Electron identification relies mainly on the electromagnetic calorimeter in the barrel region (High density Projection Chamber HPC) which is a sampling device having a relative energy resolution of $\pm 5.5\%$ for electrons with 45.6 GeV/c momentum, and a spatial resolution along the beam axis of ± 2 mm. A neural network, combining information from several detectors, has been developed for electron identification. Electrons of momentum above 3 GeV/c are identified with an efficiency of $(75 \pm 2)\%$. The misidentification probability that a pion be identified as electron is about 1.0%.

3 Event selection and simulation

Charged particles were required to have a measured momentum between 0.3 GeV/c and 50 GeV/c, a relative error on momentum less than 100%, a track length in the TPC larger than 30 cm and a distance of closest approach to the interaction point of less than 4 cm in radius and less than 10 cm along the beam axis.

Hadronic events were retained using only selected charged particles with momentum greater than 0.4 GeV/c. Five or more charged particles and a total energy in charged particles larger than 12% of the collision energy, assuming all charged particles to be pions, were required. A total of $N_{\rm Z} = 3.52$ million hadronic events was obtained from the 1992-1995 data. Simulated hadronic events were generated using the JETSET 7.3 Parton Shower program [11]. The B meson mean lifetime was set to 1.6 ps. The generated events were followed through the detailed detector simulation DELSIM [12] and then processed through the same analysis chain as the real data. The hadronic event selection efficiency was thus estimated to be $\epsilon_{\rm Z} = 95.7\%$. The data sample contained also 0.2% of τ pair events and 0.2% of Bhabha events.

In order to estimate the reconstruction efficiencies and the invariant mass resolutions, some dedicated samples of events containing a $\rm D_1^0$ or $\rm D_2^{*0}$ decaying into $\rm D^{*+}\pi^-$ were generated.

4 $\rm D^{*+}\ell^-$ selection and production rate

The $\rm D^{*+}$ candidates were reconstructed in the channels $\rm D^{*+} \to D^0\pi_*^+$ with a $\rm D^0$ decaying into $\rm K^-\pi^+$, $\rm K^-\pi^+\pi^+\pi^-$ or $\rm K^-\pi^+(\pi^0)$ where the π^0 was not reconstructed.

The primary interaction vertex was computed in space for each event using an iterative procedure based on the χ^2 of the fit. The average transverse position of the interaction point, known for each fill, was included as a constraint during the primary vertex fit. In order to increase the $\rm b\overline{b}$ purity of the selected sample, using the impact parameter of all measured charged particle tracks in the event, the probability that all tracks originate from the primary vertex was required to be smaller than 0.1 [13].

Only charged particles produced in the same direction as the lepton were considered for the reconstruction of charmed mesons. The kaon candidate in $\rm D^0$ decay was required to have the same charge as the identified lepton. The momentum of each $\rm D^0$ decay product had to be larger than 1 GeV/c, except for $\rm K^-\pi^+\pi^+\pi^-$ where the minimum momentum of candidate pions was lowered to 0.3 GeV/c. The lepton and π_* candidates, and at least two particles from the $\rm D^0$ decay were required with at least one hit in the Vertex Detector. Then a $\rm K^-\pi^+$ or $\rm K^-\pi^+\pi^+\pi^-$ vertex was computed in space. For K3π tracks, their impact parameters relative to the secondary vertex were required to be smaller than 200 μm. The apparent decay length of the $\rm D^0$ had to be positive. This distance was computed in the plane transverse to the beam axis and it was given the same sign as the scalar product of the $\rm D^0$ momentum with the vector joining the primary to the $\rm D^0$ vertices.

To reduce the combinatorial background in the $\rm K^-\pi^+\pi^+\pi^-$ and $\rm K^-\pi^+(\pi^0)$ channels, the kaon candidate was required to be identified according to the RICH and dE/dx informations. In the $\rm D^0 \to K^-\pi^+$ and $\rm D^0 \to K^-\pi^+(\pi^0)$ decay channels, the angle θ^* between the $\rm K^-\pi^+$ momentum vector and the kaon direction in the $\rm K^-\pi^+$ rest frame was required to satisfy the condition $\cos\theta^* > -0.9$. For genuine $\rm D^0$ candidates an isotropic distribution in $\cos\theta^*$ is expected whereas the background is strongly peaked in the backward direction.

Any other charged particle with a momentum between 0.3 GeV/c and 4.5 GeV/c and a charge opposite to that of the kaon was used as pion candidate of the $\rm D^{*+} \to D^0\pi_*^+$ decay. The scaled $\rm D^{*+}$ energy, $X_E(\rm D^*) = E(\rm D^*)/E_{beam}$, had to be larger than 0.15.

The lepton momentum was required to be larger than 3 GeV/c and its transverse momentum relative to the $\rm D^{*+}$ momentum vector had to be larger than 0.5 GeV/c.

These cuts reduced the fraction of leptons from $\overline{\mathrm{D}}$ semileptonic decays or τ decays. A $\mathrm{D}^0\pi_*\ell$ vertex (denoted "B" vertex in the following) is fitted in space. The momentum vectors of all these particles were recomputed at this new vertex. In order to reject fake leptons from fragmentation, either the χ^2 probability of the B vertex was required to be larger than 10^{-3} or the lepton impact parameter relative to the B vertex had to be smaller than 50 μm. Finally the B decay length was defined, as above, as the signed distance between the primary and secondary B vertices. This B decay length divided by its error was required larger than one.

Then the selection of $\mathrm{D}^{*+}\ell^-$ events relied on the small mass difference (ΔM) between the D^{*+} and the candidate D^0. Fig. 1a) shows the mass difference distribution $M(\mathrm{K}^-\pi^+\pi^+) - M(\mathrm{K}^-\pi^+)$ when the $\mathrm{K}^-\pi^+$ invariant mass is within 75 MeV/c^2 of the nominal D^0 mass. Fig. 1b) shows the invariant K3π mass distribution when the mass difference value ΔM is within 2 MeV/c^2 of the nominal D^{*+}-D^0 mass difference. Fig. 1c) shows the mass difference distribution $M(\mathrm{K}^-\pi^+\pi^+) - M(\mathrm{K}^-\pi^+)$ when the $\mathrm{K}^-\pi^+$ invariant mass is between 1550 and 1700 MeV/c^2.

A clear signal corresponding to $\mathrm{D}^{*+}\ell^-$ events is observed in each distribution (data points). In Fig. 1a) and c) the background is described by the function $a(\Delta M - m_\pi)^b$ where a and b are free parameters. The D^{*+} signals are described by Gaussian functions. The K3π mass distribution of figure 1b) is fitted by using a second order polynomial for the combinatorial background, a Gaussian function for the $\mathrm{D}^0 \to \mathrm{K}^-\pi^+\pi^+\pi^-$ events and a second Gaussian function which describes events where the kaon and pion mass of the $\mathrm{K}^-\pi^-$ candidates are permuted. According to the simulation the latter contribution amounts to 25% of the fitted signal, with a broad width of 110 MeV/c^2. For each decay channel, the mass distributions of the wrong sign $\mathrm{D}^{*+}\ell^+$ events (hatched histograms) is fitted with the same shape parameters as the right sign signal. This allows to determine the contribution of fake lepton events which will be subtracted. The number of D^{*+} observed, within the quoted range around the D^0 mass and $\mathrm{D}^{*+}-\mathrm{D}^0$ mass difference, is shown in table 2.

	Mass range (MeV/c^2)		Nb.	Nb.
D^0 decay channel	$M(\mathrm{D}^0)$	ΔM	$\mathrm{D}^{*+}e^-+\mathrm{D}^{*+}\mu^-$	$\mathrm{D}^{*+}e^++\mathrm{D}^{*+}\mu^+$
$\mathrm{K}^-\pi^+$	1790-1940	142.5-148.5	459$\pm$25	36$\pm$8
$\mathrm{K}^-\pi^+\pi^+\pi^-$	1830-1900	143.5-147.5	288$\pm$19	1^{+6}_{-1}
$\mathrm{K}^-\pi^+(\pi^0)$	1550-1700	$<$155	462$\pm$28	25$\pm$11

Table 2: Mass selections and number of D^{*+} candidates observed in each decay channel.

The $\mathrm{D}^{*+} \to \mathrm{D}^0\pi^+_*$ followed by $\mathrm{D}^0 \to \mathrm{K}^-\pi^+$ decay was selected with loose criteria. For this reason, this channel is used to normalise the absolute rate of all $\mathrm{D}^{*+}\ell^- X$ final states. According to the simulation, the average reconstruction efficiency of $\mathrm{D}^{*+}\ell^-$ events is $\epsilon_{\mathrm{D}^*\ell} = 0.166 \pm 0.003$ (MC stat.). A fraction, denoted f_{sl}, of about 92% of $\mathrm{D}^{*+}\ell^-$ events are genuine b quark semileptonic decays. The remaining is attributed to $\mathrm{D}^{*+}\tau^-$ and $\mathrm{D}^{*+}\overline{\mathrm{D}}$ events where the reconstructed lepton ℓ^- is produced from the τ^- or semileptonic $\overline{\mathrm{D}}$ decay. The semileptonic branching fraction of a b quark into $\mathrm{D}^{*+}\ell^-$ final states can

thus be measured as follows:

$$BR(\mathrm{b} \to \mathrm{D}^{*+}\ell^- X) = \frac{\epsilon_{\mathrm{Z}}}{N_{\mathrm{Z}}} \frac{1}{2R_{\mathrm{b}}} \frac{N(\mathrm{D}^{*+}e^-)_{\mathrm{K}\pi} + N(\mathrm{D}^{*+}\mu^-)_{\mathrm{K}\pi}}{2\ \epsilon(\mathrm{D}^{*}\ell)_{\mathrm{K}\pi}} \frac{f_{sl}}{BR(\mathrm{D}^{*+} \to (\mathrm{K}^-\pi^+)\pi^+)}$$
$$= (2.80 \pm 0.17\ (\mathrm{stat.}) \pm 0.20\ (\mathrm{syst.}))\% \quad (1)$$

where $R_{\mathrm{b}} = 0.2170 \pm 0.0009$ is the Z partial decay width into $\mathrm{b\overline{b}}$ events [14] and $N(\mathrm{D}^{*+}\ell^-)$ is obtained by subtracting the right sign and the wrong sign $\mathrm{D}^*\ell$ candidates in the $\mathrm{K}^-\pi^+$ channel of table 2.

The systematics are detailed in table 3. Following the detailed study of Ref. [15], a $\pm 1\%$ uncertainty is assigned to the reconstruction efficiency of each charged particle. The requirement of the Vertex Detector information has been evaluated on a large sample of exclusive D^{*+} in Z decays. The track resolution error includes the $\mathrm{D}^0\pi^+_*\ell^-$ vertex quality and decay distance selections. It was estimated by removing these cuts and by using the same D^{*+} sample. The mass resolution describes the uncertainty due to the D^0 mass and $\mathrm{D}^{*+}-\mathrm{D}^0$ mass difference selections. The uncertainty on the background level below the D^{*+} signal in figure 1 was studied in the simulation.

		$BR(\mathrm{b} \to \mathrm{D}^{**}\ell^- X)$ / $BR(\mathrm{b} \to \mathrm{D}^{*+}\ell^- X)$		
Error source	$BR(\mathrm{b} \to \mathrm{D}^{*+}\ell^- X)$	D_1^0	D_2^{*0}	all D^{**}
$\mathrm{D}^{*+}\tau^-$ background [1]	∓ 0.8	–	–	–
$\mathrm{D}^{*+}\overline{\mathrm{D}}$ background [1]	∓ 1.1	–	–	–
$BR(\mathrm{D}^{*+} \to \mathrm{D}^0\pi^+)$ [1]	∓ 2.0	–	–	–
$BR(\mathrm{D}^0 \to \mathrm{K}^-\pi^+)$ [1]	∓ 2.3	–	–	–
D^{**} mass [1]	–	$\pm$ 5.0	$\mp$ 7.6	–
D^{**} width [1]	–	± 14.4	± 23.0	–
lepton identification	± 1.4	–	–	–
track reconstruction	± 4.0	$\pm$ 1.0	$\pm$ 1.0	± 1.0
VD requirement	± 0.8	$\pm$ 1.0	$\pm$ 1.0	± 1.0
track resolution	± 1.3	$\pm$ 3.3	$\pm$ 3.3	± 3.1
mass resolution	± 1.0	$\pm$ 3.4	$\pm$ 2.7	–
MC statistics	± 1.9	$\pm$ 1.1	$\pm$ 1.1	± 1.1
background estimate	± 3.9	–	–	± 7.0
π_{**} momentum cut	–	$\pm$ 1.0	$\pm$ 1.0	± 1.0
Total	± 7.2	± 16.1	± 24.7	± 7.9

Table 3: Relative systematic uncertainties (%) on the $\mathrm{D}^{*+}\ell^-$ production rates and $\mathrm{D}^{**}\ell^-$ fractions.

5 Semileptonic b decay into narrow orbital state

In this section, a search for the narrow D_1^0 and D_2^{*0} particles decaying into $\mathrm{D}^{*+}\pi^-$ is performed. Due to their better mass resolution, only the $\mathrm{K}\pi$ and $\mathrm{K}3\pi$ decay modes of the D^0 are used. In the next section a search for both narrow and wide D^{**} will be presented,

based on the impact parameter distribution of the π_{**} candidate relative to the primary interaction vertex and using all three D^0 decay channels.

In the $D^{*+}\pi^-_{**}$ final state, all particles of charge opposite to the D^{*+} and momentum greater than 0.5 GeV/c were considered. The invariant $D^{*+}\pi^-_{**}\ell^-$ mass had to be smaller than 5 GeV/c^2. The π_{**} track was required to have at least 2 hits in the Vertex Detector. Its combined RICH and dE/dx information had not to be compatible with the kaon hypothesis. The impact parameter of this π_{**} relative to the previously measured $D^{*+}\ell^-$ vertex had to be less than 100 μm.

For each π_{**} candidate, the impact parameter relative to the primary interaction vertex was computed in the plane transverse to the beam axis. The sign of this impact parameter is defined with respect to the $D^*\ell$ direction. It is positive if the intercept between the π_{**} and the $D^*\ell$ momentum vectors is downstream of the primary vertex along the $D^*\ell$ direction, and negative if it is upstream [13]. In order to reject almost half of the background due to fragmentation particles, the impact parameter relative to the primary vertex had to be positive. According to the simulation, only 6% of π_{**} candidates did not satisfy this requirement.

To estimate the $M(D^{*+}\pi^-)$ invariant mass, the following mass difference was computed: $M(D^{*+}\pi^-) = M(D^0\pi^+_*\pi^-) - M(D^0\pi^+_*) + m_{D^*}$ where m_{D^*} is the nominal D^{*+} mass [1]. This gives a resolution σ of about 5 MeV/c^2 on $M(D^{*+}\pi^-)$, according to the simulation.

The $M(D^{*+}\pi^-)$ invariant mass distribution is presented in figure 2 for the selected $D^{*+}\pi^-\ell^-$ events (data points). It is fitted as the sum of three contributions: a background function of the form $\alpha(M(D^*\pi) - m_{D^*} - m_\pi)^\beta \cdot \exp(-\gamma(M(D^*\pi) - m_{D^*} - m_\pi))$ where m_π is the pion mass and α, β and γ are free parameters; for each D_1^0 and D_2^{*0} resonance, the convolution of a Breit-Wigner function and a Gaussian describing the experimental mass resolution. Fixing the mass and width of both resonances to their world average value [1], 26.7 ± 8.2 D_1^0 and 14.8 ± 7.7 D_2^{*0} are fitted. The χ^2/DOF is 23.6/38. The mass distribution of the wrong sign $D^{*+}\pi^-\ell^+$ events (hatched histogram) is fitted with the same shape parameters as the right sign signal: only 0.6 ± 3.1 D_1^0 and 5.4 ± 4.1 D_2^{*0} are found in this sample. The fraction of b semileptonic decays into the narrow resonances is then obtained as follows:

$$\frac{BR(b \to D^{**}\ell^- X)\; BR(D^{**} \to D^{*+}\pi^- X)}{BR(b \to D^{*+}\ell^- X)} \;=\; \frac{N(D^{**}\ell^-)}{\epsilon(\pi_{**})\; N(D^{*+}\ell^-)} \qquad (2)$$

where $\epsilon(\pi_{**}) = 0.55$ is the π_{**} reconstruction and selection efficiency obtained from the simulation, and $N(D^{**}\ell^-)$ is the fitted number of candidates in the right sign sample. As no significant signal is observed for the D_2^{*0}, only the result obtained for the D_1^0 is given:

$$\frac{BR(b \to D_1^0\ell^- X)\; BR(D_1^0 \to D^{*+}\pi^-)}{BR(b \to D^{*+}\ell^- X)} = 0.068 \;\pm\; 0.021 \text{ (stat.)} \;\pm\; 0.011 \text{ (syst.)}\,. \qquad (3)$$

The systematics are detailed in table 3. The mass and width of the narrow D^{**} were varied within their measured values [1]. The mass spectrum was also fitted with a mass resolution of 5 ± 1 MeV/c^2. No background uncertainty is assigned for the narrow D^{**} because it is fully included in the statistical error of the fitted background parameters. The other systematics are common to those detailed in the next section where all narrow and wide D^{**} are considered.

6 Semileptonic b decays into any charm excited state

The same selection criteria as above are applied for the search of π_{**} candidates from all narrow and wide D^{**} states. Without any cut on the π_{**} impact parameter relative to the primary vertex, the π_{**} reconstruction and selection efficiency is $\epsilon(\pi_{**}) = 0.59$.

The π_{**} impact parameter distribution of simulated B semileptonic decays is shown in figure 3a). Compared with charged particles produced in b quark fragmentation or gluon radiation in jets (see figure 3b), π_{**} from $b \to D^{**}\ell^-\bar{\nu}_\ell$ decays present a long tail at large impact parameters. The shape of the π_{**} signal is fitted with the sum of a Gaussian plus the convolution of a Gaussian and an exponential function. The shape of the fragmentation tracks is fitted with the sum of two Gaussian functions.

For real data $D^{*+}\pi^-_{**}\ell^-$ events, the impact parameter distribution is shown in figure 4a). Two sources of background were subtracted:

- Fake D^{*+} associated to a true lepton ℓ^-: this combinatorial background was estimated by using events in the tails of the mass distributions of figure 1, after a proper normalisation to the fraction of events below the D^{*+} signal.

- True D^{*+} associated to a fake lepton ℓ^-: this background is due to charged pions and kaons misidentified as leptons. It was subtracted by using the π^-_{**} candidates produced in the same hemisphere as a wrong sign $D^{*+}\ell^+$ event (shown in the hatched histograms of figure 1).

All the remaining events can be attributed to b semileptonic decays into $D^{*+}\ell^-$ final state. The π^-_{**} candidates are thus either true tracks from D^{**} decays or particles from jet fragmentation. The shapes of these two contributions were parametrised from the simulation (see figure 3). Figure 4a) is fitted, letting free the normalisation of the two components. The χ^2/DOF is 34.4/21. A total amount of 111 ± 16 π_{**} candidates are measured, from which the following overall $D^{**} \to D^{*+}\pi^-_{**}$ fraction is inferred:

$$\frac{BR(b \to D^{**}\ell^- X)\ BR(D^{**} \to D^{*+}\pi^-_{**}X)}{BR(b \to D^{*+}\ell^- X)} = 0.165\ \pm\ 0.024\ (\text{stat.})\ \pm\ 0.013\ (\text{syst.}) \quad (4)$$

which significantly improves a previous DELPHI measurement [6].

The systematics are detailed in table 3. As a cross-check of the procedure, the impact parameter of wrong sign π^+_{**} tracks is shown in figure 4b). A similar fit gives 8 ± 5 wrong sign $D^{*+}\pi^+_{**}\ell^-$ events. This small excess could be partly attributed to D^{**} decays into $D^*\pi\pi$, or remaining particles from $D^*\overline{D}$ final states. Conservatively, a relative systematic uncertainty of $\pm 7\%$ is taken into account for this residual background effect. In the data, fitting the wrong sign spectrum with a Gaussian function gives a mean impact parameter which is 25 ± 7 μm larger than in the simulation. A similar shift of the fragmentation shape in the fit of the right sign spectrum would decrease the number of fitted $D^{*+}\pi^-_{**}\ell^-$ events by only 6%. This variation is smaller than the quoted systematic uncertainty of $\pm 7\%$.

The track resolution uncertainty describes the cut on the π_* impact parameter with respect to the B vertex: the upper limit on the impact parameter was varied between 50 μm and 200 μm (corresponding to a π_{**} reconstruction efficiency of 0.42 and 0.68, respectively). A small dependance on the π_{**} momentum cut was observed when varying the minimum value between 0.5 GeV/c and 1.5 GeV/c.

7 Summary and conclusion

Assuming all $D^{*+}\pi^-\ell^-$ events to originate from B^- semileptonic decays and neglecting $\overline{B} \to D^*\pi\pi\ell^-\bar{\nu}_\ell$ decays, the B^- semileptonic branching fraction into D^{**0} final state can be obtained. The probability for a b quark to fragment into a B^-, $f_{B^-} = 0.40 \pm 0.02$ [1], will be used in the following.

According to isospin conservation, neglecting decays into $D^{(*)}\pi\pi$ or $D^{(*)}\rho$, the branching fraction $BR(D_1^0 \to D^{*+}\pi^-) = 2/3$ is estimated. From equations (1) and (3), the B^- semileptonic branching fraction into the D_1^0 narrow orbital state is thus obtained:

$$BR(B^- \to D_1^0\ell^-\bar{\nu}_\ell) \;=\; (0.72 \;\pm\; 0.22\ (\text{stat.}) \;\pm\; 0.13\ (\text{syst.}))\ \% \ .$$

More data would be necessary to estimate the B^- semileptonic branching fraction into D_2^{*0}.

The B^- semileptonic branching fraction into narrow and wide $D^{*+}\pi^-$ final states is inferred from equations (1) and (4):

$$BR(B^- \to D^{*+}\pi^-\ell^-\bar{\nu}_\ell X) = (1.15 \;\pm\; 0.17\ (\text{stat.}) \;\pm\; 0.14\ (\text{syst.})\ \% \ .$$

These results agree with previous LEP and CLEO measurements (see table 4).

BR (%)	CLEO [4]	OPAL [3]	ALEPH [2]	DELPHI
$b \to D^{*+}\ell^- X$		2.87 ± 0.29		2.80 ± 0.26
$B^- \to D_1^0\ell^-\bar{\nu}_\ell$	0.56 ± 0.16	$2.11 \pm 0.94 \pm 0.11$	$0.70 \pm 0.15 \pm 0.04$	$0.72 \pm 0.25 \pm 0.04$
$B^- \to D_2^{*0}\ell^-\bar{\nu}_\ell$	< 0.8 (90% CL)		< 0.61 (95% CL)	
$B^- \to D^{*+}\pi^-\ell^-\bar{\nu}_\ell X$			$1.18 \pm 0.24 \pm 0.06$	$1.15 \pm 0.21 \pm 0.06$
$\overline{B} \to D\pi\ell^-\bar{\nu}_\ell \;+\; D^*\pi\ell^-\bar{\nu}_\ell$			2.14 ± 0.42	

Table 4: Comparison of the measured semileptonic branching fractions. The statistical and systematic errors have been added quadratically. For LEP data the second error, due to f_{B^-}, is common to the three experiments. Note that these results slightly differ from Ref. [1] due to the new f_{B^-} value.

Acknowledgements

We are greatly indebted to our technical collaborators and to the funding agencies for their support in building and operating the DELPHI detector, and to the members of the CERN-SL Division for the excellent performance of the LEP collider.

References

[1] Particle Data Group, C. Caso et al., "Review of Particle Properties", Euro. Phys. J. **C3** (1998) 1.

[2] ALEPH collab., D. Buskulic et al., Zeit. Phys. **C73** (1997) 601.

[3] OPAL collab., R. Akers et al., Zeit. Phys. **C67** (1995) 57.

[4] CLEO collab., A. Anastassov et al., Phys. Rev. Lett. **80** (1998) 4127.

[5] DELPHI collab., P. Abreu et al., Zeit. Phys. **C74** (1997) 19;
DELPHI collab., P. Abreu et al., Zeit. Phys. **C76** (1997) 579.

[6] DELPHI collab., P. Abreu et al., Zeit. Phys. **C71** (1996) 539.

[7] N. Isgur and M.B. Wise, Phys. Rev. Lett. **66** (1991) 1130 and ref. therein.

[8] S. Godfrey and R. Kokoski, Phys. Rev. **D43** (1991) 1679.

[9] DELPHI collab., P. Abreu et al., Nucl. Instr. & Meth. **A378** (1996) 57.

[10] DELPHI collab., V. Chabaud et al., Nucl. Instr. & Meth. **A368** (1996) 314.

[11] T. Sjöstrand, Comp. Phys. Comm. **39** (1986) 347;
T. Sjöstrand and M. Bengtsson, Comp. Phys. Comm. **43** (1987) 367;
T. Sjöstrand, JETSET 7.3 manual, CERN-TH 6488/92 (1992).

[12] DELSIM Reference Manual, DELPHI 87-98 PROG 100, Geneva, July 1989, unpublished.

[13] G. Borisov and C. Mariotti, Nucl. Instr. & Meth. **A372** (1996) 181.

[14] The LEP Collaborations ALEPH, DELPHI, L3, OPAL, the LEP Electroweak Working Group and the SLD Heavy Flavour Group, "A Combination of Preliminary LEP Electroweak Measurements and Constraints on the Standard Model", prepared from Contributions to the 1997 summer conferences, preprint CERN–PPE/97–154 (1997), unpublished.

[15] DELPHI collab., P. Abreu et al., Phys. Lett. **B425** (1998) 399.

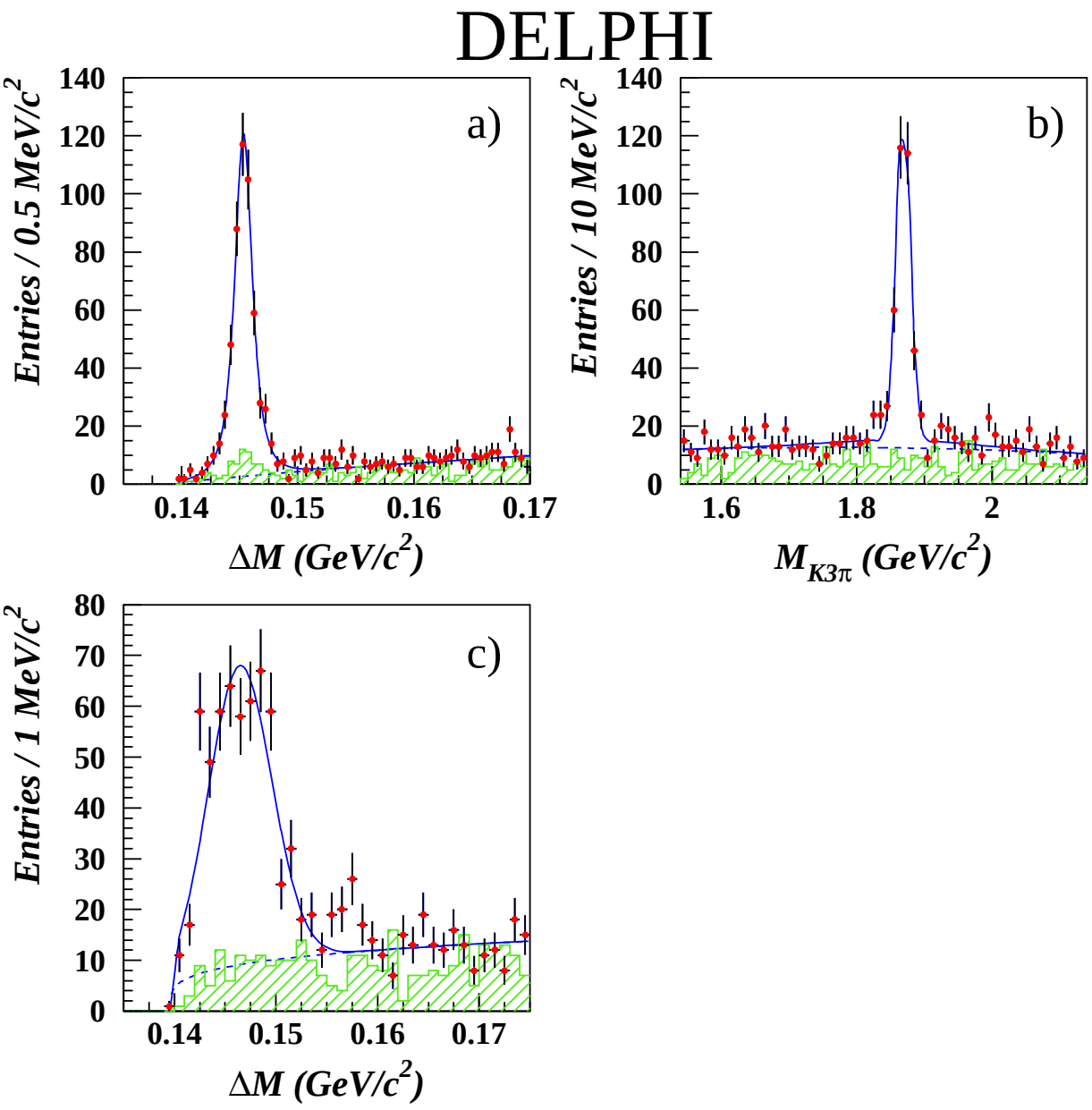

Figure 1: (a) and (c) Mass difference distributions in the the $D^{*+} \to (K^-\pi^+)\pi_*^+$ and $D^{*+} \to (K^-\pi^+(\pi^0))\pi_*^+$ decay channels; (b) invariant mass distribution of the D^0 from $D^{*+} \to (K^-\pi^+\pi^+\pi^-)\pi_*^+$ decay. Right charge $D^{*+}\ell^-$ (dots) and wrong charge $D^{*+}\ell^+$ (hatched histogram) events are shown. The solid line curve is a fit which includes a background parametrisation (dashed curve alone) and Gaussian functions for the signal (see section 4).

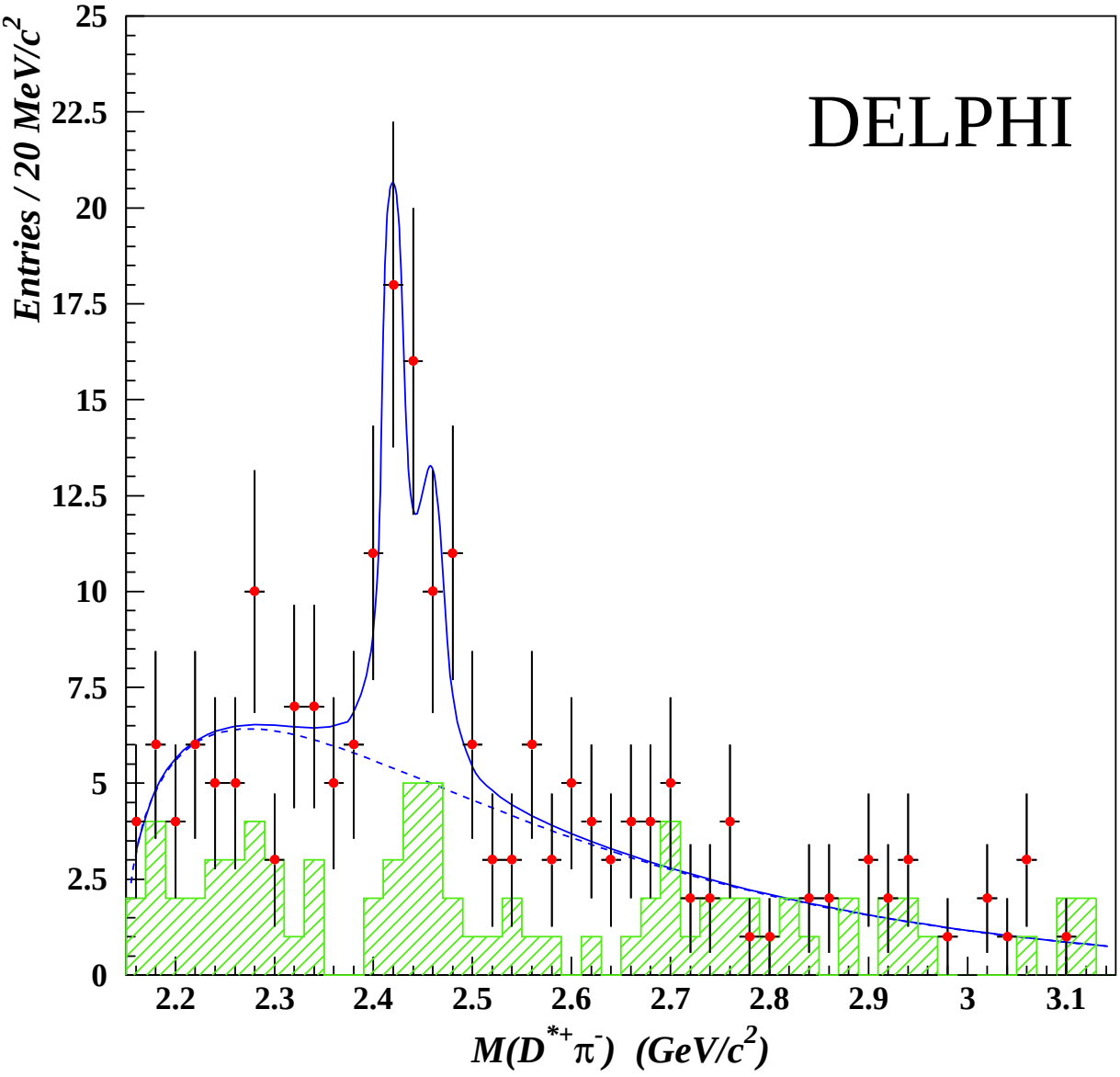

Figure 2: Invariant mass distribution $M(\mathrm{D}^{*+}\pi^-)$ of $\mathrm{D}^{*+}\pi^-\ell^-$ events (data points). The mass computation is explained in the text. The solid line curve is a fit which includes a background parametrisation (dashed curve alone) and two Breit-Wigner convoluted with a Gaussian function (see section 5). The wrong sign $\mathrm{D}^{*+}\pi^-\ell^+$ candidates are shown in the hatched histogram.

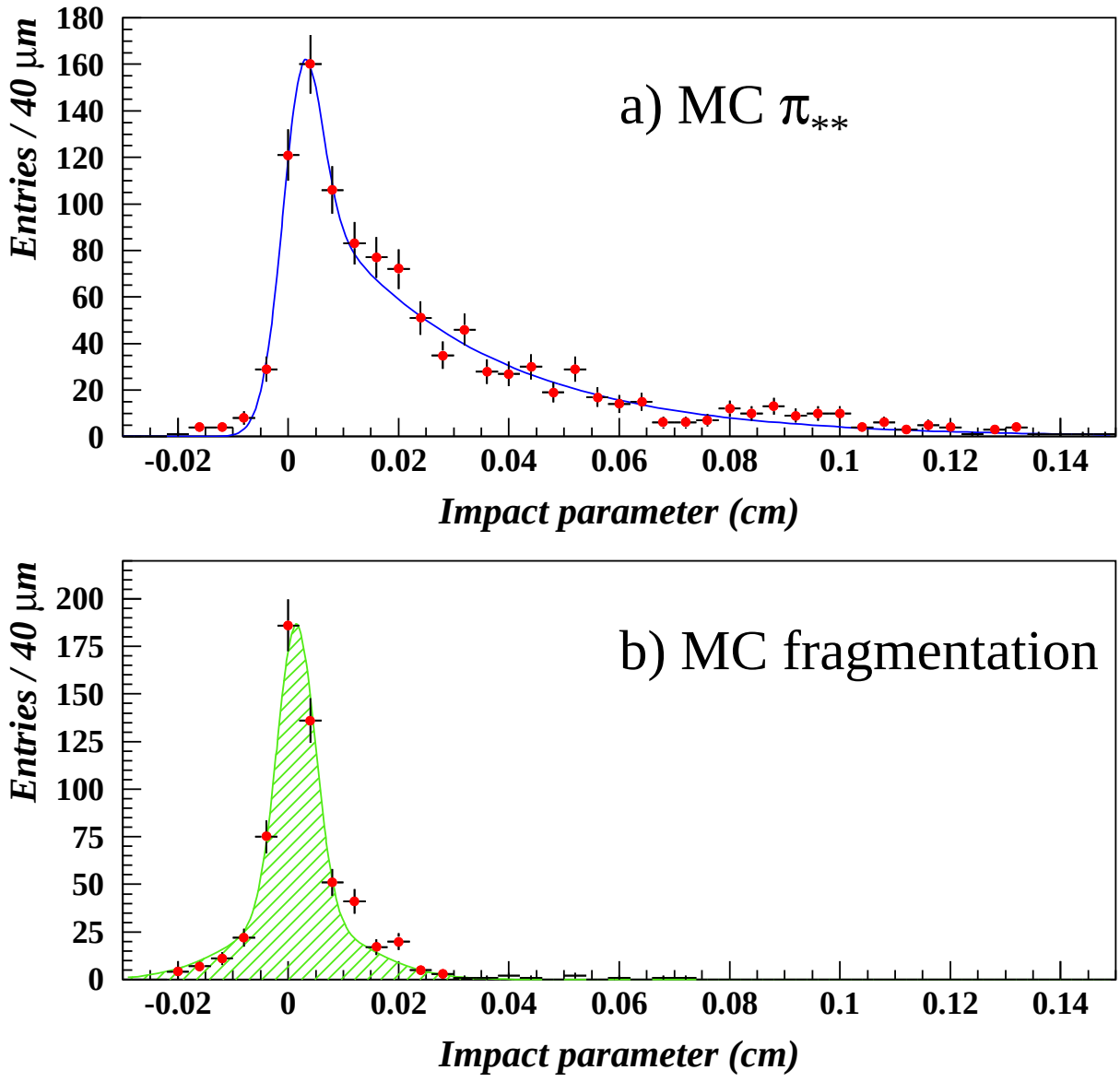

Figure 3: Impact parameter relative to the primary interaction vertex in simulated B semileptonic decays for a) π_{**} from D** decay and b) charged particles from jet fragmentation. The curves are fitted functions (see section 6).

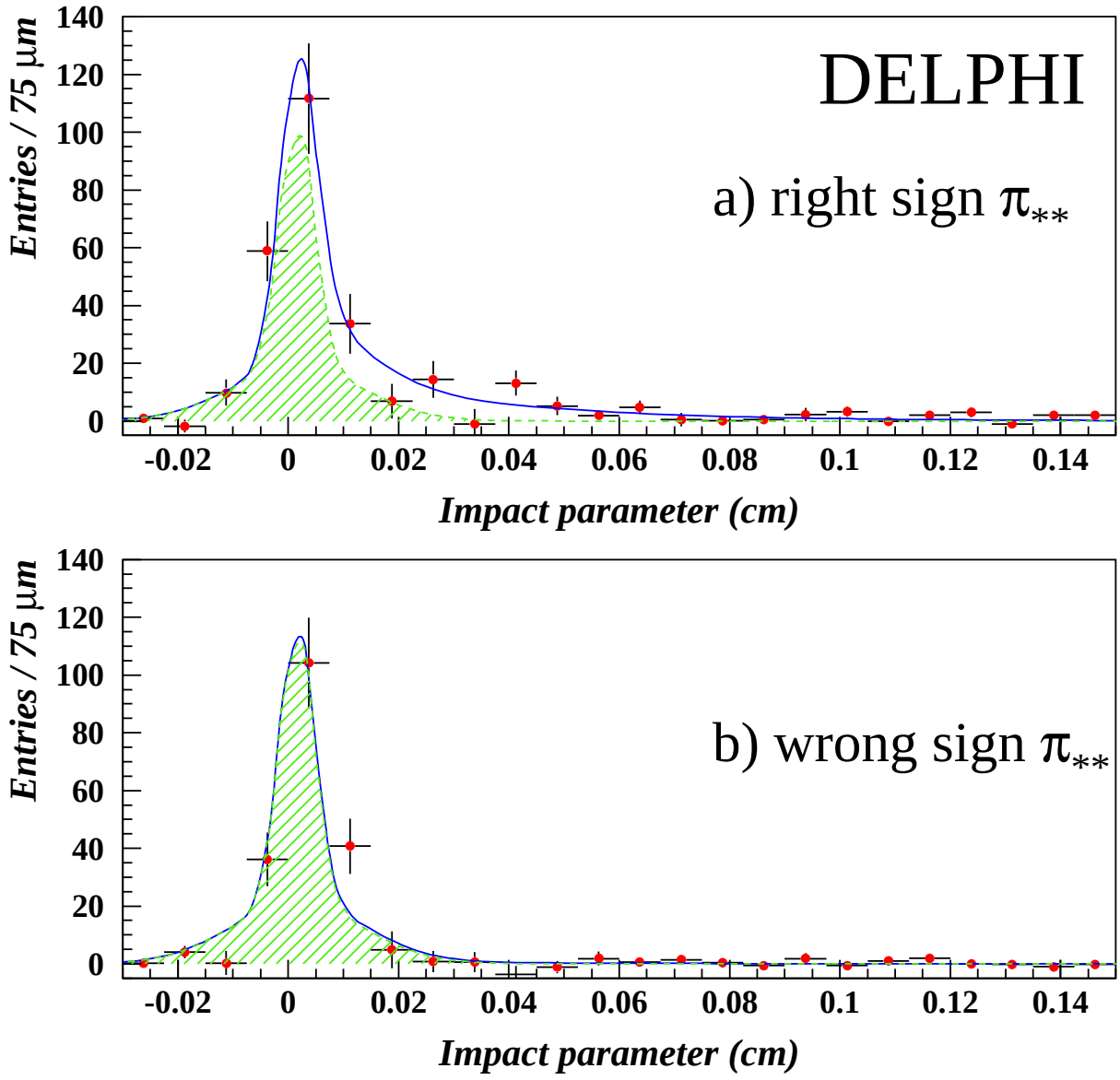

Figure 4: Impact parameter relative to the primary interaction vertex in real data for a) right charge π^-_{**} and b) wrong charge π^+_{**} candidates. The hatched area is the contribution from jet fragmentation. The solid line curve is the result of a fit which includes a parametrisation of fragmentation and π_{**} from D^{**} decays (see section 6).